Machine learning based soil maps for a wide range of soil properties for the forested area of Switzerland

Andri Baltensweiler [a,*], Lorenz Walthert [a], Marc Hanewinkel [b], Stephan Zimmermann [a], Madlene Nussbaum [c]

[a] *Swiss Federal Institute for Forest, Snow and Landscape Research WSL, Birmensdorf, Switzerland*
[b] *Chair of Forestry Economics and Forest Planning, University of Freiburg, Freiburg, Germany*
[c] *School of Agricultural, Forest and Food Sciences HAFL, Bern University of Applied Sciences BFH, Zollikofen, Switzerland*

ARTICLE INFO

ABSTRACT

Spatial soil information in forests is crucial to assess ecosystem services such as carbon storage, water purification or biodiversity. However, spatially continuous information on soil properties at adequate resolution is rare in forested areas, especially in mountain regions. Therefore, we aimed to build high-resolution soil property maps for pH, soil organic carbon, clay, sand, gravel and soil density for six depth intervals as well as for soil thickness for the entire forested area of Switzerland. We used legacy data from 2071 soil profiles and evaluated six different modelling approaches of digital soil mapping, namely lasso, robust external-drift kriging, geoadditive modelling, quantile regression forest (QRF), cubist and support vector machines. Moreover, we combined the predictions of the individual models by applying a weighted model averaging approach. All models were built from a large set of potential covariates which included e.g. multi-scale terrain attributes and remote sensing data characterizing vegetation cover.

Model performances, evaluated against an independent dataset were similar for all methods. However, QRF achieved the best prediction performance in most cases (18 out of 37 models), while model averaging out-performed the individual models in five cases. For the final soil property maps we therefore used the QRF predictions. Prediction performance showed large differences for the individual soil properties. While for fine earth density the R^2 of QRF varied between 0.51 and 0.64 across all depth intervals, soil organic carbon content was more difficult to predict ($R^2 = 0.19$–0.32). Since QRF was used for map prediction, we assessed the 90% prediction intervals from which we derived uncertainty maps. The latter are valuable to better interpret the predictions and provide guidance for future mapping campaigns to improve the soil maps.

1. Introduction

Forest soils provide a wide range of crucial ecosystem services such as carbon storage, water cycle regulation and water filtering, wood production and biodiversity (Guo et al., 2001; Greiner et al., 2017; Pereira et al., 2018). Assessing these services has become increasingly important due to climate change (e.g. changes in tree species composition, biomass production and carbon stocks (Lal, 2005; Bréda et al., 2006; McDowell et al., 2020)), natural hazards (Hümann et al., 2011), biodiversity loss (Hartmann et al., 2012; Motiejūnaitė et al., 2019) or soil erosion (Hartanto et al., 2003). Therefore, spatially explicit information about soil properties such as pH, texture, organic carbon content or soil thickness is required. However, soil information is often only available for a subarea of the desired region or only described as broad soil series at a coarse scale. In Switzerland, for example, the legacy Swiss Soil Suitability Map (SSSM) at the scale of 1:200,000 (Swiss Federal Statistical Office, 2001) was used for forest species distribution modelling (SDM) e.g. by Camathias et al. (2013) as no more detailed maps of Swiss forest soils were available. This coarse scaled map contains data collected mainly in agricultural areas with focus on agricultural soil suitability that have limited information on forest soils. Understanding the ecological requirements that determine, for example, the distribution of tree species is a prerequisite for sustainable forest management. This requires knowledge of ecological conditions, such as the spatial distribution of edaphic information. Therefore, recent studies on SDM have emphasised that more effort should be made to derive covariates

---

such as soil pH and nutrients reflecting local edaphic conditions to improve SDM predictions (Mod et al., 2016; Scherrer and Guisan, 2019; Buri et al., 2020).

Digital soil mapping (DSM) has been proven to be a useful approach to create maps of spatially continuous soil properties applying the 'scorpan' (soil, climate, organisms, relief, parent material, age and space) model (e.g. McBratney et al., 2003; Minasny and McBratney, 2016). Similar to SDMs, in the 'scorpan' model a relationship between field (soil) observations and environmental factors is established. However, unlike data on the occurrence of forest plant species, the availability of soil data in forested areas over large geographical extents is often limited, mainly due to high acquisition costs and time-consuming laboratory work (Grunwald et al., 2011). In combination with a not optimally distribution of the soil samples over the feature space and a high spatial variation of soil, which is particularly the case in mountainous regions due to e.g. heterogeneous topography and geology (Ballabio, 2009; Hoffmann et al., 2014; Simon et al., 2020), the accurate prediction of soil properties is challenging. To tackle this challenge, different model structures are compared to choose a single 'best' model or 'best' model set to improve prediction accuracy by reducing the variance of predicted values (Hastie et al., 2009). Machine learning methods such support vector machines (SVM), k-nearest neighbours (kNN), cubist or random forest (RF) are evaluated and the best performing one is used to make the prediction (e.g. Gomes et al., 2019; Keskin et al., 2019; Mahmoudzadeh et al., 2020). However, depending on the environmental conditions, quantity and distribution of soil samples, one model approach can lead to a more accurate prediction in a given area than others and vice versa (Diks and Vrugt, 2010; Guevara et al., 2018; Taghizadeh-Mehrjardi et al., 2019). Therefore, the concept of model averaging (MA) was introduced. The idea is to combine predictions from different approaches that model differently structured relationships between response (dependent variable) and covariates. The combination of several predictions into a single one likely reduces the variance of the averaged model by balancing the errors of the single models and consequently results in a better fit and more robust prediction (Araujo and New, 2007; Tebaldi and Knutti, 2007; Abbott, 2014). Various recent DSM studies implemented such a MA approach, e. g., for predicting pH, soil texture, soil organic matter, soil water storage capacity and soil types (Malone et al., 2014; Román Dobarco et al., 2017; Nussbaum et al., 2018; Caubet et al., 2019; Taghizadeh-Mehrjardi et al., 2019; Chen et al., 2020). In these studies, model averaging often, but not always, improved predictive performance.

The spatial representation of uncertainty in soil maps belongs to the fundamental principles of DSM and is therefore a crucial aspect when predicting soil properties (McBratney et al., 2003). In geostatistical models, the quantitative estimation of the uncertainty was a by-product and uncertainty maps were provided to users together with the soil maps (Vaysse and Lagacherie, 2017). A common way to visualize the uncertainty of a spatial prediction is to map the upper and lower limit of the 90% prediction interval (PI). The PI reports the range of values within which the true value is expected to occur 9 times out of 10, with a 1 out of 20 probability for each of the two tails (Arrouays et al., 2014). Computing such intervals for machine learning predictions can be done by non-parametric bootstrapping techniques (Davison and Hinkley, 1997) where models are repeatedly fitted to randomly resampled subsets of the data. The versatile approach of bootstrapping was used to create prediction intervals for regression tree based models (Padarian et al., 2017; Thomas et al., 2015; Viscarra Rossel et al., 2015), for gradient boosted trees (Hamzehpour et al., 2019), for shrinkage type regression (Liddicoat et al., 2015) or for convolutional neuronal networks (Wadoux, 2019). Bootstrapping allows to combine uncertainties of several models, e.g. when random forest predictions are combined with a subsequent kriging of residuals (Szatmári and Pásztor, 2019). As a special case, quantile regression forest (QRF; Meinshausen, 2006) uses the model inherent bootstrap aggregation procedure (Hastie et al., 2009) of random forest to quantify uncertainties directly from the model fit (Vaysse and Lagacherie, 2017; Dharumarajan et al., 2020). Besides resampling based bootstrap approaches, uncer tainties in machine learning have been quantified by quantile regression applied to nested cross-validation predictions (Kasraei et al., 2021) or the Monte Carlo dropout, a Bayesian optimization approach for neuronal networks (Gal and Ghahramani, 2016). Another versatile approach to empirically quantify uncertainties for machine learning predictions is based on partitioning the environmental factors. Covariate space is divided by (fuzzy) clustering and accompanying local uncertainties are assigned to the predictions belonging to the same cluster (Malone et al., 2011; Malone et al., 2014).

In DSM, terrain attributes (TAs) are the most widely used covariates because topography is an important soil forming factor and digital elevation models (DEMs) are readily available to derive TAs (e.g. McBratney et al., 2003). Topography influences pedogenesis and thus soil properties through its effects on geomorphological, hydrological and biogeochemical processes (Creed et al., 2002; Seibert et al., 2007). These processes have a strong scale dependency (Cavazzi et al., 2013; Maynard and Johnson, 2014) operating at landscape scales (Grinand et al., 2008; Kim and Zheng, 2011) but also at local scales in submeter ranges (Baltensweiler et al., 2017; Baltensweiler et al., 2020). To incorporate various spatial scales, a multi-scale terrain analysis was suggested (Grinand et al., 2008; Behrens et al., 2010). Such a multi-scale approach improved prediction of soil types and properties compared to using only single-scale TAs (Behrens et al., 2010; Miller et al., 2015; Baltensweiler et al., 2020).

Large sets of potentially relevant covariates are now available for DSM studies, not only because of the implementation of multi-scale terrain analysis (Behrens et al., 2010; Miller et al., 2015), but also due to the advent of high-resolution remote sensing data to describe e.g. vegetation cover or land use (Mulder et al., 2011), the availability of a wide range of climatic variables (Liddicoat et al., 2015) as well as the derivatives of geological and legacy soil maps (Nussbaum et al., 2014). Although such large sets of covariates may contain partly multi-collinear environmental data, they facilitate to find the relevant predictors to build the DSM models (Nussbaum et al., 2018). Many recent DSM studies, however, used a relatively small set of covariates, with less than 30 predictors included (e.g. Vaysse and Lagacherie, 2015; Mulder et al., 2016; Yang et al., 2016; Liu et al., 2020; Simon et al., 2020). Brungard et al. (2015) found that complex models using covariates identified by recursive feature selection were more accurate in predicting soil classes than models using covariates selected by soil scientists. Integrating a large number of covariates, however, seems advantageous regarding model performance (Nussbaum et al., 2018; Ågren et al., 2021; Petermann et al., 2021).
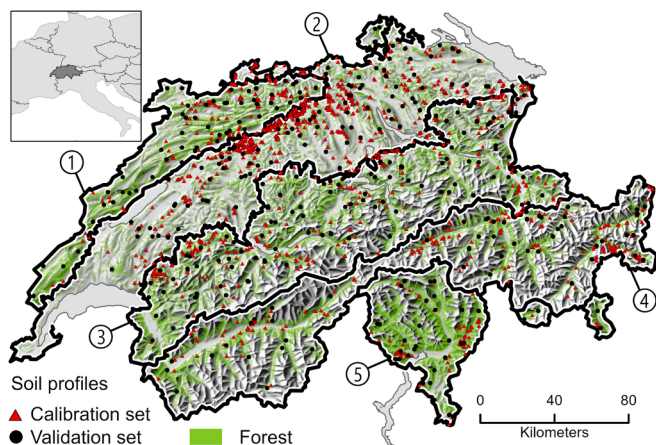

Fig. 1. Location of the 2071 soil profiles (calibration and validation set) within the forested area of Switzerland. (1) Jura Mountains, (2) Central Plateau, (3) Northern Alps, (4) Central Alps, (5) Southern Alps.

The main objective of this study was to build high-resolution soil property maps for the entire forested area of Switzerland. We aimed to predict six soil properties (pH, soil organic carbon, clay, sand, gravel and soil density) for six soil depths (between 0 and 200 cm) as well as soil thickness (entity of all soil depths), resulting in a total of 37 target variables (responses). To efficiently predict this large number of responses, our goal was to build models with minimal human intervention. We used large sets of covariates as input into six modelling approaches that all build different covariate-response relationships. We applied MA because we expected to reduce the prediction variance compared to the individual models. The predictive performance of all models was evaluated with independent data. For the predictions calculated by the QRF, we derived accompanying uncertainty maps for each response.

2. Materials and methods

2.1. Study area

The study area represents the forested area of Switzerland (circa 45–47°N and 6–10°E), which covers roughly 30% of the country (13,000 km^2; Brändli et al., 2020; Fig. 1). Due to the high variability of climate, geology and topography, Switzerland has strong environmental gradients within small distances. Forests extend over altitudes from 190 to 2300 m a.s.l. (Brändli et al., 2020) and tree species composition varies along this altitudinal gradient. The climatic conditions vary considerably within the forested area: the mean annual temperature varies from −1 to 13 °C and mean annual precipitation ranges from 600 to 2900 mm (MeteoSwiss, 2020). The geologic parent material for soil formation is often limestone or dolomite in the Jura Mountains and in parts of the Alps and Pre-Alps. In the Central Plateau fluvioglacial sediments of several Quaternary glaciations and of the Tertiary are widespread, while igneous and metamorphic rocks are common in the Southern Alps and in parts of the Central Alps. This large variation of soil forming factors results in a high diversity of forest soils across Switzerland (Walthert et al., 2004).

2.2. Soil data

We used data of 2071 soil profiles acquired in various soil surveys between 1968 and 2012 to build the models. Most of the profiles were collected by the Swiss Federal Institute for Forest, Snow and Landscape Research WSL (1412), some by various cantons (537; Mosimann, 2004-2010) or the research institute Agroscope (122) (Walthert et al., 2015). The soil profile density was 0.05 and 0.17 profiles per km^2 in relation to the entire and the forested area of Switzerland, respectively. The location of the soil profiles was chosen by purposive sampling according to the aims of the various soil surveys. Therefore, the spatial distribution of the profiles was heterogeneous with clusters of profiles e.g. in the Central Plateau and sparse data in some mountainous regions (Fig. 1).

We predicted the following six soil properties: gravel content [vol%], clay content [wt%], sand content [wt%], density of the fine soil fraction (≤ 2 mm) [g cm^{-3}], pH [−] and soil organic carbon (SOC) content [wt %]. These properties were assessed for genetic soil horizons and had to be transferred to soil depths of fixed width (Nussbaum et al., 2018) as we used the following six standard depths of the GlobalSoilMap.net specification (Arrouays et al., 2014): 0–5, 5–15, 15–30, 30–60, 60–100 and 100–200 cm. The values of all genetic horizons within a given depth interval were summed in a weighted manner, where the weighting took into account the depth fraction, the fine-earth density, and the stone content of the corresponding genetic horizons. Due to the different data sources, tailored harmonisation procedures and quality checks were required to provide a consistent soil dataset. The gravel content (mineral particles >2 mm) in the soil pit was estimated in the field as volumetric percentage, sometimes in classes. The three texture classes clay (< 0.002 mm), silt (0.002–0.05 mm) and sand (0.05–2 mm) were determined from 2-mm sieved soil samples either with the sedimentation

method (Gee et al., 1986) or estimated in the field with a finger probe (AK SK, 2016). The density of the fine soil fraction (particles ≤ 2 mm) was measured on a selection of soil profiles by use of 559 volumetric samples mainly taken with steel cylinders (1000 m^3) from mineral soil horizons. Based on this data set, Nussbaum et al. (2016) developed a linear regression pedotransfer function to estimate density in all soil profiles. Soil pH was measured potentiometrically in a suspension of 2-mm sieved soil samples in 0.01 M CaCl$_2$. SOC content was determined in milled soil samples with seven different measurement techniques. For most of the samples from the cantonal profiles, the Walkley-Black method was used and for most of the WSL profiles, SOC content was analyzed by combustion of the samples with a CN analyzer NC 2500 (CE Instruments, Italy) whereby any existing carbonates were removed by HCl vapor prior to combustion (Walthert et al., 2010). For 184 soil samples SOC content was derived from soil color by use of the Munsell color code.

For soil thickness prediction, we defined total soil depth [cm] as reaching down to a non-root-permeable layer or solid rock. If neither a non-permeable layer nor solid rock was encountered within the depth of the profile, the excavation depth of the profile pit was used. Soil thickness was limited in 5% of the soils by a non-permeable layer and in 11% by solid rock. 84% of the profiles had no visible depth limitation within the profile, so that in these cases soil thickness is not known. Soil thickness must therefore be interpreted as minimal expected soil thickness.

2.3. Calibration and validation datasets

The soil profiles were split into a calibration set (82%) and a validation set (18%) to compute the model performance statistics (Supplementary Table S1). Not every soil property was assessed in every soil profile and in some cases soil data was not available for all six depth layers. Therefore, the number of 2071 soil samples per soil depth represent the maximum, with no missing values for a given target variable and soil depth layer.

To ensure that the validation points represented well the different soil forming conditions we sampled validation points per physiographic unit of the Swiss soil suitability map (SSSM; Swiss Federal Statistical Office, 2001). The number of profiles per SSSM unit was

$$n_{unit} = 0.25 * n_{tot} * A_{unit} / A_{total} \qquad (1)$$

where A_{unit} = forest area in a given physiographic unit, A_{total} = the sum of the forest area in all units, n_{tot} = total number of soil profiles within all units and 0.25 = set value for the portion of validation points for each unit. The number of soil profiles was not proportionally distributed to the forested area per unit and some units had few profiles only. If the number to be sampled in a unit n_{unit} was larger than 25% of the actual number of profiles in this unit, then 25% of the actual number of profiles was used. To avoid overrepresentation of validation points in clusters with a high profile density, validation points were sampled (without replacement) with probability weights corresponding to the forest area in the Voronoi polygons (Supplementary Fig. S1).

2.4. Environmental covariates

We built a comprehensive set of environmental covariates to describe the most important soil forming factors defined in the scorpan model (McBratney et al., 2003). All covariates were prepared as raster datasets with a resolution of 5 m × 5 m, regardless of the original resolution.

2.4.1. Topography

Using the Python API of ArcGIS (v.10.3, ESRI) and SAGA GIS (v2.1.2), a large number of terrain attributes (TAs) were derived based on two different Digital Elevation Models (DEMs) with a resolution of 5

and 25 m (Swisstopo, 2020). To include various spatial scales, we applied 2D convolution filters with a Gaussian weighting scheme to smooth the TAs. The filters were defined as circles with different radii: for the 5 m TAs, radii of 15, 30 and 60 m were applied, for the 25 m TAs 50, 100 and 200 m were used. The calculation of the TAs was based on the following main computational functions: convexity, curvature, flow accumulation, flow length, flow path, slope, specific catchment area, ruggedness, stream power, topographic position index (TPI), topographic wetness index (TWI) and valley depth. TPI was derived after Jenness (2011), the TWI was calculated with the single-flow direction algorithm according to O'Callaghan and Mark (1984) as well as with the multiple flow direction algorithm according to Freeman (1991).

2.4.2. Parent material, soil legacy information and landscape types

No detailed information on parent material was available for the extent of the Swiss forest. We therefore used two overview maps to describe the geology: the Geotechnical Map (map scale 1:200,000, 18 classes; Bundesamt für Landestopografie, 1967) and the Hydrogeological Map (map scale 1:500,000, 9 classes; Swisstopo, 2007). To broadly partition the Swiss forested area into areas with similar pedogenetic and geological conditions, we used the large-scaled Swiss Soil Suitability Map (SSSM, map scale 1:200,000; Swiss Federal Statistical Office, 2001). The SSSM contains soil-land units defined on the basis of strongly aggregated geomorphological and pedological criteria. We supplemented the SSSM with information from the Geological Map of Switzerland and the map of the last Glacial Maximum (map scale 1:500,000; Swisstopo, 2009) resulting in a total of 30 classes (Nussbaum et al., 2014). In addition, the SSSM contains a finer classification with 144 map units corresponding to second level soil series. We supplemented these units with 10,865 data points of pH topsoil samples taken in forested areas throughout Switzerland (Swiss National Forest Inventory LFI, 1984). As these legacy data were found to be unreliable in several cases due to survey inconsistencies and laboratory sample processing errors, we assigned the median pH values within a given SSSM unit and assigned these pH values to the respective unit. Furthermore, we used two overview maps that classify Switzerland into 10 biogeographic regions (map scale 1:200,000; Gonseth et al., 2001), and 38 landscape types (map scale 1:200,000; Bundesamt für Raumentwicklung, 2016).

2.4.3. Climate

We used three climate datasets on mean annual and monthly temperature and precipitation, cloud cover, sunshine duration, radiation and potential evapotranspiration. The datasets were based on different spatial resolutions and on different periods: 25 m resolution, 1961–1990 (Zimmermann and Kienast, 1999); 100 m, 1981–1990 (Frehner et al., 2011), and 250 m and 2 km, 1981–2010 and 1975–2010 (MeteoSwiss, 2020). Because it was not a priori clear which data set was most appropriate, we used all three as covariates in the statistical analysis.

2.4.4. Vegetation

To capture the potential influence of the vegetation on the soil properties we calculated various vegetation indices. Based on Sentinel-2 satellite images (10 m resolution, level 1C; Drusch et al., 2012) covering the vegetation period of 2015 to 2018, we derived the Normalized Vegetation Index (NDVI; Rouse et al., 1974), the Pigment Specific Simple Ratio (PSSRa; Blackburn, 1998) and Green Normalized Difference Vegetation Index (GNDVI; Gitelson et al., 1996). To consider a longer time span we also calculated an averaged NDVI raster over the summer months for the years 1985–2015 based on Landsat-5 images (30 m resolution; Masek et al., 2006). To further account for vegetation we derived a terrain corrected canopy height model (resolution 25 m) from LIDAR data (Swisstopo, 2020) which describes the height of the forest cover. Both the vegetation indices and the canopy height model are proxies for forest productivity. We further included the proportion of coniferous and deciduous trees as a proxy for litter input (Waser et al., 2017).

2.4.5. Final set of potential covariates for model building

For the non-spatial models (LASSO, cubist, RF, SVM, see Section 2.5.1), we included north and east coordinates besides the environmental covariates. Coordinate axes were additionally rotated by 30° and 60° to allow for trend modelling in intermediate cardinal directions (Møller et al., 2020). To account for possible variation of the data over the long sampling period we added the sampling year as covariate. Predictions were made for the last observed year (2012). Strongly positive skewed covariates were transformed by natural logarithm to avoid unstable model fits for approaches with non-robust loss functions (lasso, geoGAM, cubist, RF). Some covariates centred around zero (e.g. curvature) with long tails on either side. We log-transformed the absolute values of each side of the distribution separately re-adding the sign after transformation.

To avoid multi-collinearity in the final set of covariates, we removed highly correlated covariates with a Pearson correlation coefficient $|r| > 0.8$. This finally led to 88 covariates representing topography, 52 with a climate information, 18 characterizing vegetation and 14 representing parent material, soil legacy information and landscape types. With the normal and rotated coordinates for the non-spatial models and the sampling year we started model building for each modelling method with 178 covariates.

2.5. Methods

2.5.1. Modelling methods

We used three different statistical modelling methods, namely least absolute shrinkage and selection operator (lasso), robust external-drift kriging (georob), geoadditive modelling (geoGAM) as well as three machine learning procedures: random forest (RF), cubist and support vector machines (SVM). The machine learning methods were chosen for having satisfactory performance (Nussbaum et al., 2018) and being of different nature, hence possibly covering different relations between responses and covariates. The first four model methods were described in detail in Nussbaum et al. (2018). Cubist and SVM have been successfully used in DSM for predicting various soil properties (Brungard et al., 2015; Viscarra Rossel et al., 2015; Mulder et al., 2016). For all methods, except RF, we identified the optimal tuning parameters by calculating the root mean square error (RMSE, Eq. (4)) for the 10-fold cross-validation using the same cross-validation subsets.

RF is widely used in DSM studies and is known to achieve good predicting performance (Hengl et al., 2018; Gomes et al., 2019; Keskin et al., 2019). Tuning parameters for RF are the number of trees n_{tree}, the minimal number of observations at terminal nodes n_{min} and the number of randomly chosen covariates m_{try} to test at each split. According to Hastie et al. (2009; p. 288ff) RF performs remarkably well with little tuning, which also has been shown in DSM studies (Spiess, 2016; Camera et al., 2017; Nussbaum et al., 2018). We therefore used default values for the number of trees ($n_{tree} = 500$) and the minimal number of observations at terminal nodes ($n_{min} = 5$) for all RF fits (R package randomForest, Liaw and Wiener, 2002). To reduce the large number of covariates we applied sequential recursive backward elimination (Kuhn and Johnson, 2013) based on node-impurity covariate importance (Hastie et al., 2009). To speed up computation, we removed 5 to 10 covariates at each step fitting models with 168, 158, …, 108, 103, …, 8, 3 covariates. Correlated covariates might substitute each other in the set of m_{try} candidates selected to test for binary splitting. As a result, the set of covariates after recursive backward elimination is often strongly correlated. To additionally reduce the covariates we applied an ad-hoc decorrelation procedure that was performing similarly to a more complex approach based on principal component analysis (Hertzog, 2017). The rows of the correlation matrix of the remaining covariates were compared. With pairwise differences above a threshold ε along the complete row the covariates were considered correlated and only the covariate with the largest importance was retained. Optimal ε was determined by minimizing out-of-bag RMSE (Eq. (4)). For covariate
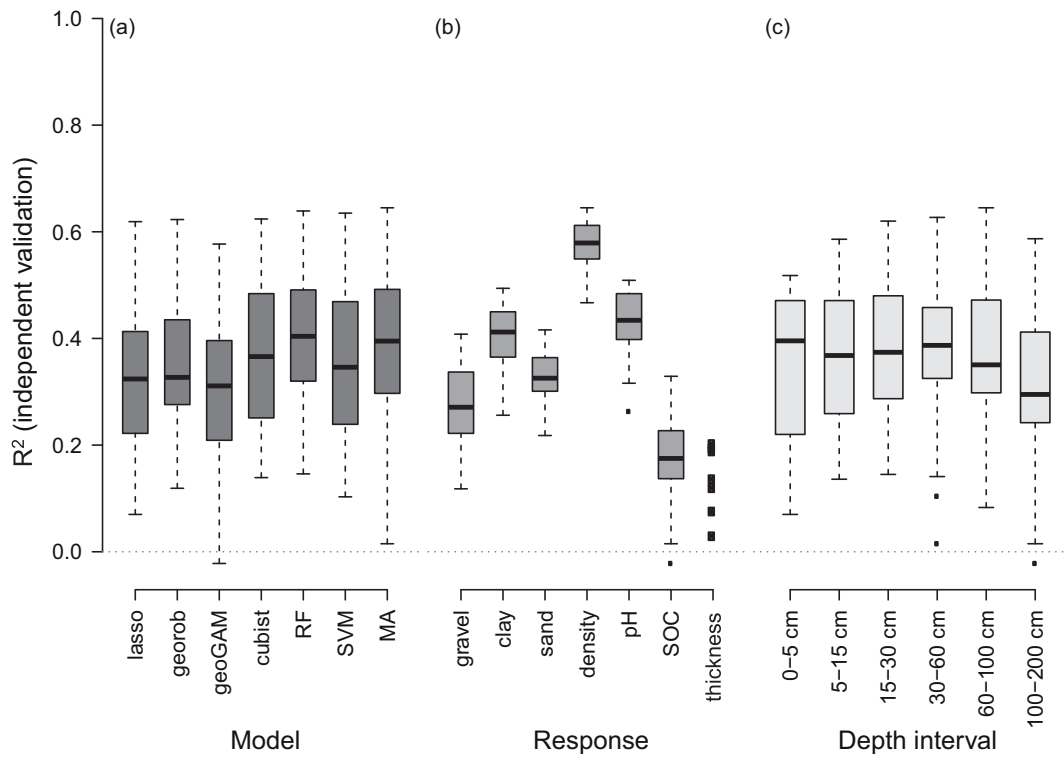
Fig. 2. Boxplots of R^2 (for independent validation data) grouped by method (a), response type (b) and soil depth (c). Boxplots in: (a) summarize R^2 values of $n = 37$ responses per method (6 soil properties for 6 soil depth intervals and for soil thickness), (b) $n = 42$ responses per response type and (c) $n = 36$ responses per soil depth interval. For the response type soil thickness (b) R^2 values are individually shown for the $n = 7$ models. Abbr.: lasso: grouped least absolute shrinkage and selection operator, georob: robust external-drift kriging, geoGAM: boosted geoadditive model, cubist: rule-based regression, RF: random forest, SVM: support vector machines, MA: model averaging.

removal we used as a default $m_{try} = p/3$. To find optimal m_{try} for the final covariate set we minimized out-of-bag RMSE by iterating through $m_{try} = 1, 2, .., p$.

2.5.2. Response transformation

For the parametric methods lasso, georob and geoGAM we transformed positively skewed responses $Y(s)$. Suitable response transformation was chosen based on a profile plot of the Box-Cox transformation parameter λ (Box and Cox, 1964). Transformation by square root (sqrt) was applied to SOC content while the other responses were not transformed.

Predictions of sqrt-transformed data were unbiasedly back-transformed by:

$$\widetilde{Y}(s) = \widehat{f}(x(s))^2 + \widehat{\sigma}^2 - \mathrm{Var}\left[\widehat{f}(x(s))\right] \qquad (2)$$

with $\widehat{f}(x(s))^2$ being the prediction of the sqrt-transformed response, $\widehat{\sigma}^2$ the estimated residual variance of the fitted model and $\mathrm{Var}\left[\widehat{f}(x(s))\right]$ the variance of $\widehat{f}(x(s))$ as provided by the final model. Predictions by lasso were back-transformed by $(\cdot)^2$ because $\mathrm{Var}\left[\widehat{f}(x(s))\right]$ was not known.

Responses for RF, cubist and SVM were not transformed. Clay and sand contents were modelled independently. Silt was computed as the remainder to 100%.

2.5.3. Model averaging (MA)

To combine the prediction of the six different modelling methods into one single prediction we applied a weighting scheme based on the performance of the individual models. The weights were computed proportional to the inverse cross-validation (CV) or out-of-bag mean squared error (MSE). We refrained from optimising weighting schemes as an additional test set was not available. The calibration data was used

up to this step to find optimal tuning parameters by repeated CV and to calibrate the final model for each of the six modelling approaches. Hence, different weighing schemes for MA by comparing CV errors lacked independent calibration (Chen et al., 2020) and tests were inconclusive.

2.5.4. Assessment of model performance

The predictive model performance of the seven DSM methods (including MA) was quantified by comparing predicted $\widetilde{Y}(s_i)$ and observed $Y(s_i)$ soil properties for all locations s_i of the independent validation data set (see Section 2.3). The bias (Eq. (3)) was used to quantify systematic under- or overestimation, which should be close to zero for any reasonable DSM product. The RMSE (Eq. (4)) was calculated to assess prediction accuracy. To measure the proportion of variation explained we used R^2 computed as mean squared error skill score (SS$_{mse}$, Wilks, 2011, p. 359, Eq. (5)), interpreted with R$^2 = 1$ for a perfect prediction, R$^2 = 0$ if the prediction has the same variance as the data of the validation set and R$^2 < 0$ if the prediction has a larger variance than the validation data.

$$\mathrm{bias} = -\frac{1}{n}\sum_{i=1}^{n}\left(Y(s_i) - \widetilde{Y}(s_i)\right) \qquad (3)$$

$$\mathrm{RMSE} = \left(\frac{1}{n}\sum_{i=1}^{n}\left(Y(s_i) - \widetilde{Y}(s_i)\right)^2\right)^{1/2} \qquad (4)$$

$$\mathrm{R2} = \mathrm{SS}_{mse} = 1 - \frac{\sum_{i=1}^{n}\left(Y(s_i) - \widetilde{Y}(s_i)\right)^2}{\sum_{i=1}^{n}\left(Y(s_i) - \frac{1}{n}\sum_{i=1}^{n}Y(s_i)\right)^2} \qquad (5)$$

2.5.5. Spatial prediction and uncertainty estimation

For the spatial prediction of soil properties, all covariates were gridded to a 5 m cell size, which corresponds to the maximum resolution of the predictors. However, since the final soil maps were created with a resolution of 25 m, only every fifth pixel was considered for prediction.

To quantify uncertainty for each predicted pixel, non-parametric bootstrap technique (Davison and Hinkley, 1997) has been shown to be useful for numerous machine learning methods (Liddicoat et al., 2015; Thomas et al., 2015; Viscarra Rossel et al., 2015; Padarian et al., 2017; Hamzehpour et al., 2019) and methods combinations (Szatmári and Pásztor, 2019). Here, we calculated uncertainties only for the method with the best model performance, namely RF (see Section 3.2) and used the quantile regression forest (QRF) method (Meinshausen, 2006; Vaysse and Lagacherie, 2017) which retains all observations that fall in the terminal tree nodes for all fitted trees and therefore allows to assess the conditional distributions for each prediction. We derived the 90%-prediction intervals (PI) by computing the $\alpha = 0.05$ and 0.95 quantiles using the R package quantregForest (Meinshausen, 2017). The accuracy of the 90%-PIs was assessed by the ratio of validation observations outside of the intervals computed with the calibration dataset. If less than 10% of the validation observations were outside the PIs, the intervals were too pessimistic, i.e. uncertainty was overestimated, if more than 10% were outside the PIs, the intervals were too optimistic (uncertainty was underestimated). To assess the local uncertainty of the QRF models we used accuracy plots (Goovaerts, 2001) comparing the nominal coverage probability of the validation observations with the estimated prediction intervals. The width of the 90% PI computed by the QRF was used to map the spatial patterns of uncertainty.

3. Results and discussion

3.1. Summary statistics of measured soil properties

All measured soil properties showed a high variability reflecting the high variation of soil forming factors in the study region (Supplementary Tables S2 for descriptive statistics of untransformed soil properties). In the soil depth of 5–15 cm, for example, the sand content varied from 2 to 89% and pH ranged between 2.8 and 7.8. For both soil properties, the interquartile range (IQR) tended to increase with soil depth (Supplementary Tables S2). For gravel, clay and sand content as well as for soil density and SOC content the validation set showed a larger IQR over all soil depths than the calibration set.

3.2. Validation of model performance

In general, the model performances were low to intermediate. The differences between methods were small (Fig. 2a, Supplementary Table S3). For 18 out of 37 responses, RF had most often the largest R^2. MA outperformed the single models for five responses. Georob, cubist and SVM had the largest R^2 for seven, five and two responses, respectively, while LASSO and geoGAM never performed best. GeoGAM, aiming to generate sparse and interpretable models, showed most often the lowest R^2, namely in 17 out of 37 responses. Although with only slightly larger R^2, RF was the most successful method, even better than the MA approach. Previous DSM studies showed that MA improved model performance for some but not all soil properties (e.g. Román Dobarco et al., 2017; Nussbaum et al., 2018; Chen et al., 2020). Nussbaum et al. (2018), who used a similar set of methods and the same MA scheme as in this study, showed that out of 48 modelled soil properties, MA had the best performance in 23 responses, while RF was the best performing single model in 14 cases. However, the differences in model performance were rather small ($< 0.05\%$ in terms of R^2) as also seen here. The better performance of RF compared to other methods found in the present study is in line with previous DSM analysis that have compared different model methods to predict various soil properties or
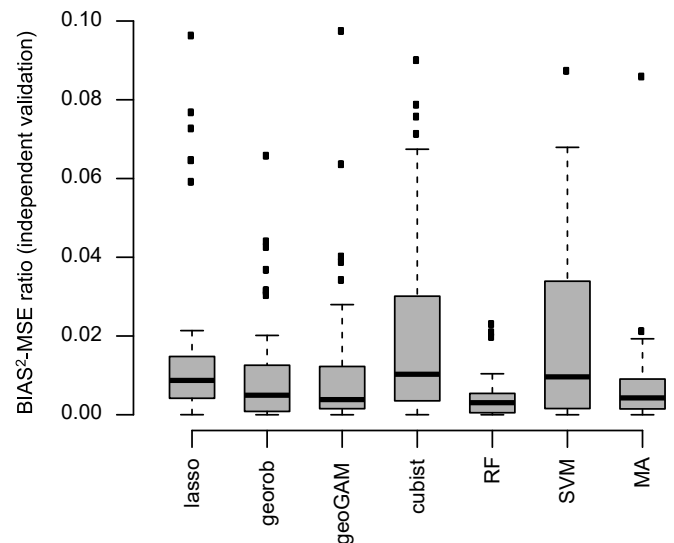

Fig. 3. Boxplots of bias^2-to-MSE-ratio for the independent validation data grouped by method. Boxplots summarize ratios of n = 37 predicted soil properties.

soil classes (e.g. Heung et al., 2017; Assami and Hamdi-Aissa, 2019; Mahmoudzadeh et al., 2020).

Because of the small differences in model performances, the weights used to calculate MA were balanced and showed a narrow dispersion (Supplementary Table S4). The smallest weight had geoGAM (0.136) and the largest weight had georob (0.195) both for SOC at 100–200 cm depth.

The performances based on the external validation dataset depended largely on the predicted soil property (Fig. 2b, Supplementary Table S3). SOC content and soil thickness were difficult to predict: based on RF predictions, which were best for 5 of the 6 soil depths, R^2 for SOC content ranged from 0.19 to 0.32. The median over all soil depths and methods was 0.17. The best validation of the soil thickness resulted in a R^2 of 0.20 achieved by cubist. To improve the prediction of soil thickness in future, parametric survival approaches (e.g. Wei, 1992) that handle the right-censored nature of the data should be further investigated. The performance values for texture were larger: for clay, sand, and gravel, the median R^2 were 0.41, 0.32, and 0.27, respectively. The high R^2 for fine earth density was most likely influenced by the pedotransfer function (PTF) also applied to the calibration and validation data (Nussbaum et al., 2016). The pH models showed the best performance at 30–60 cm depth with an R^2 of 0.50 achieved by RF while the median R^2 over all methods and depths was 0.43 (Fig. 2b, Supplementary Table S3). Opposed to previous studies (Vaysse and Lagacherie, 2015; Mulder et al., 2016; Nussbaum et al., 2018) we found no clear decrease in model performance over all soil properties with increasing soil depth (Fig. 2c). The bias was mostly small and for none of the models was its square above 10% of the MSE (Fig. 3). RF and the thereof influenced MA approach clearly showed the lowest bias whereas the largest bias was found for cubist and SVM.

Furthermore, we evaluated whether the six modelling methods tended to overfit the data. For that, we compared R^2 calculated with 10-fold cross-validation or out-of-bag (OBB, RF) with the R^2 obtained using the independent validation set for the different soil properties and depth intervals (Fig. 4). GeoGAM (Fig. 4c) was most prone to overfitting, especially for the soil properties with the lowest model performance (SOC, soil thickness, gravel) which is, although downweighted, also reflected in MA (Fig. 4g). SOC content showed the greatest variance across all methods and was partially underfitted in the independent validation for some depth intervals (Fig. 4b, d). This may be attributed to differences between the calibration and validation datasets (see Section 3.1). Lasso revealed the lowest tendency of overfitting, which has also
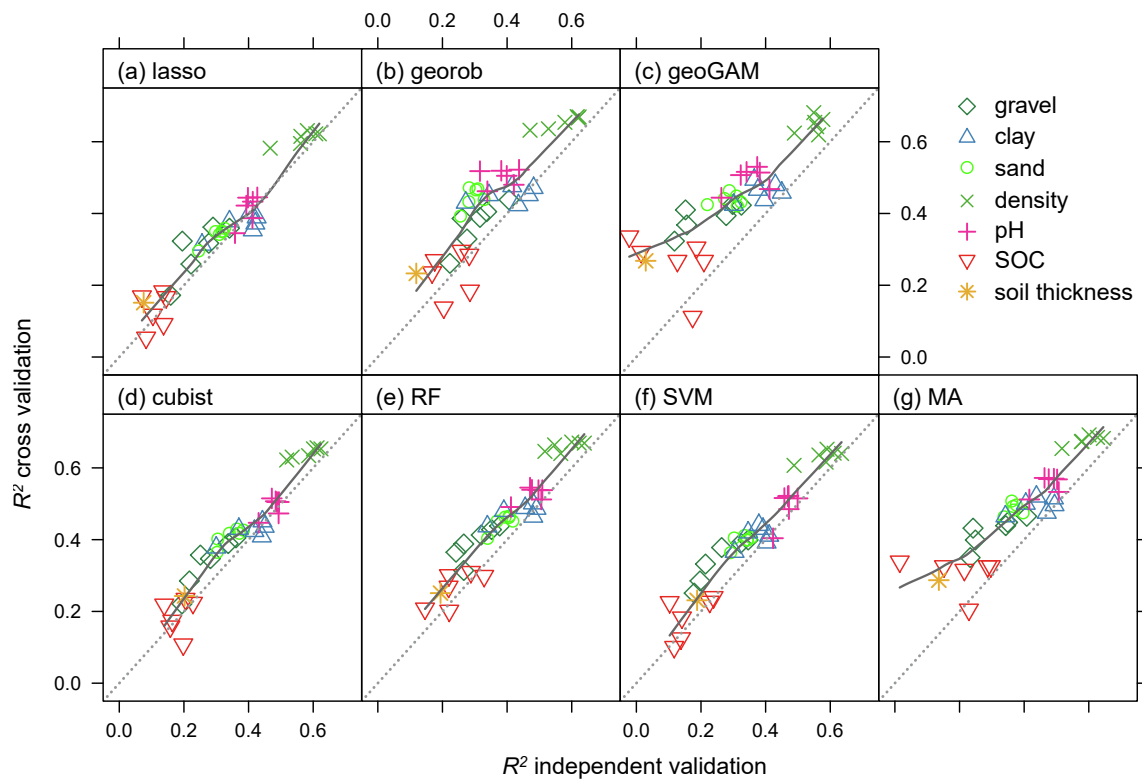
Fig. 4. R[2] calculated by both 10-fold cross-validation and independent validation grouped by method (a–g). The different data points per soil property represent the soil depth intervals. The dotted line represents the 1:1 line.

been found in previous studies (Fig. 4a, Liddicoat et al., 2015; Nussbaum et al., 2018).

We decided to use RF models for predicting soil properties since this method showed the best overall performance in terms of explained variation, had the smallest bias of all methods, and was not prone to overfitting.

3.3 Importance of covariates.

For each soil property we assessed the relative importance of covariates using the RF algorithm, aggregated the values for different covariate classes and calculated the average over all soil depths (Fig. 5). The classes comprise soil legacy information, climate, vegetation, relief, parent material and spatial position including geographic regions. For gravel, pH, SOC and soil thickness, relief was the most important class. Important covariates of this class were based on both unsmoothed TAs with 5 m resolution and TAs with 25 m resolution smoothed with large Gaussian filters. These different resolutions and filter sizes represent different spatial scales. Soil legacy information was most important to predict soil density, position/regions contributed most to predict clay and sand content. The latter covariate class includes spatial position, e.g. latitude and longitude, as well as information on geographic regions and landscape types. This class describes both spatial trends and regionalisation and is probably also a proxy for missing fine-scale geological information. Sampling year, included in the category soil legacy information, was not among the top 10 covariates for any soil property, but was selected for pH, SOC, clay and density in some of the models (8 out of 37 in total).
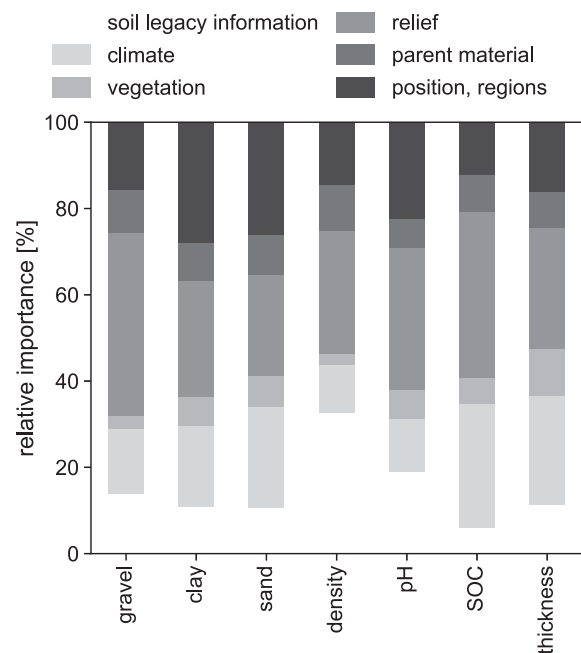

Fig. 5. Relative importance of environmental covariates in random forest aggregated over soil depths and covariates classes.

Table 1

Percentage [%] of validation observations outside of the 90%-prediction intervals for each soil property and soil thickness (10%: prediction intervals are exactly representing uncertainty, <10%: prediction intervals are too wide/uncertainty overestimated, > 10%: prediction intervals are too narrow/uncertainty underestimated.)

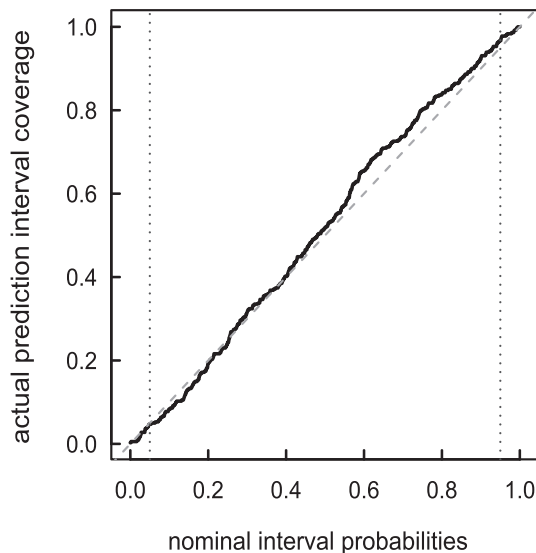| Depth [cm]	0–5	5–15	15–30	30–60	60–100	100–200
Gravel [%]		4.0	7.8	6.4	4.4	6.2	6.9
Clay [%]		11.4	11.1	10.1	9.9	13.9	13.3
Sand [%]		9.4	9.1	7.5	9.6	13.2	16.6
Density [g cm^{-3}]		11.2	10.9	12.5	6.8	9.7	8.9
pH		5.8	8.2	7.4	7.5	6.2	7.4
SOC [%]		12.2	11.5	11.4	8.8	7.8	7.9
Soil thickness [cm]	10.7						

Fig. 6. Quantile regression forest (QRF) accuracy plot for pH in 5–15 cm depth computed with the independent validation set.

3.3. Uncertainty assessment

The uncertainty for clay over all soil depths was underestimated as shown by the coverage probability computed with the independent validation set (Table 1). For sand and SOC, the uncertainty was overestimated in the upper and lower soil layers, respectively. For gravel and pH, uncertainties were overestimated across all soil depths. Nevertheless, the accuracy plot for pH in 5–15 cm depth shows that QRF predicted accurately, as the coverage probability was close to the 1:1 line (Fig. 6). However, there was a slight overestimation for probability values between 0.6 and 0.8.

3.4. Random forest pH map and spatial pattern of uncertainty

As mentioned in Section 3.2, based on model evaluations (predictive performance, bias, overfitting) across all responses as well as preference for simpler models over more complex ones, we used the RF predictions for the final soil property maps. Using RF also had the advantage that we could use the computationally efficient PIs of QRF to create uncertainty maps to accompany the soil maps. As an example, we present and discuss here the pH soil map predicted for the 5–15 cm soil depth interval because of its high relevance for many ecological studies. The pH
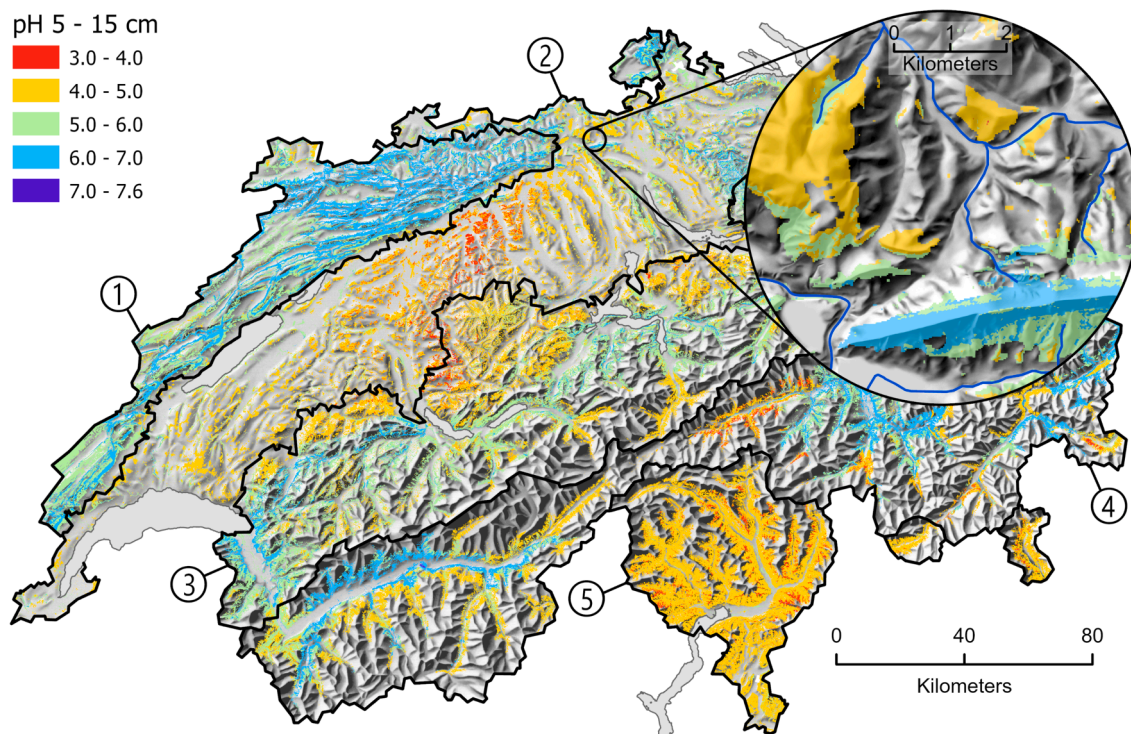

Fig. 7. Random forest pH prediction at 5–15 cm soil depth for the forested area of Switzerland, including an inset map showing the fine-scale pH distribution. (1) Jura Mountains, (2) Central Plateau, (3) Northern Alps, (4) Central Alps, (5) Southern Alps.
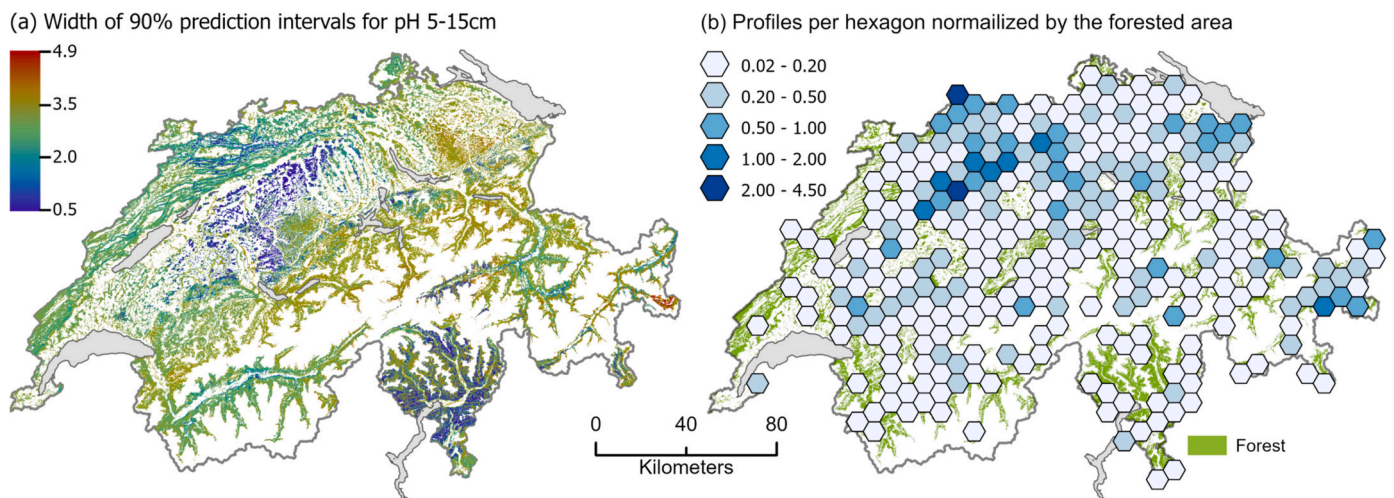
(a) Width of 90% prediction intervals for pH 5-15cm

(b) Profiles per hexagon normailized by the forested area

Fig. 8. Uncertainty map for the pH predicted for 5–15 cm soil depth (a) and aggregated density map of soil profiles (b). Uncertainty is based on the width of the 90% prediction intervals using quantile regression forest and is expressed in pH units. The aggregated density map reflects the number of calibration soil profiles per km^2 forested area within a hexagon (interhexagon distance is 10 km). If no hexagon is present, there were no calibration points within this area.

Width of 90% prediction intervals for pH 5 -15 cm

Classes of the Swiss Soil Suitability Map

Soil profiles

- U — Alpine limestone mountains
- Uv — Sedimentary rocks (Verrucane) consisting of quartz conglomerates
- V — Alpine crystalline mountains of hard bedrock (granite, orthogneiss)
- W — Alpine crystalline mountains of relatively easily weathered bedrock (paragneiss)
- R — Narrow alpine valleys

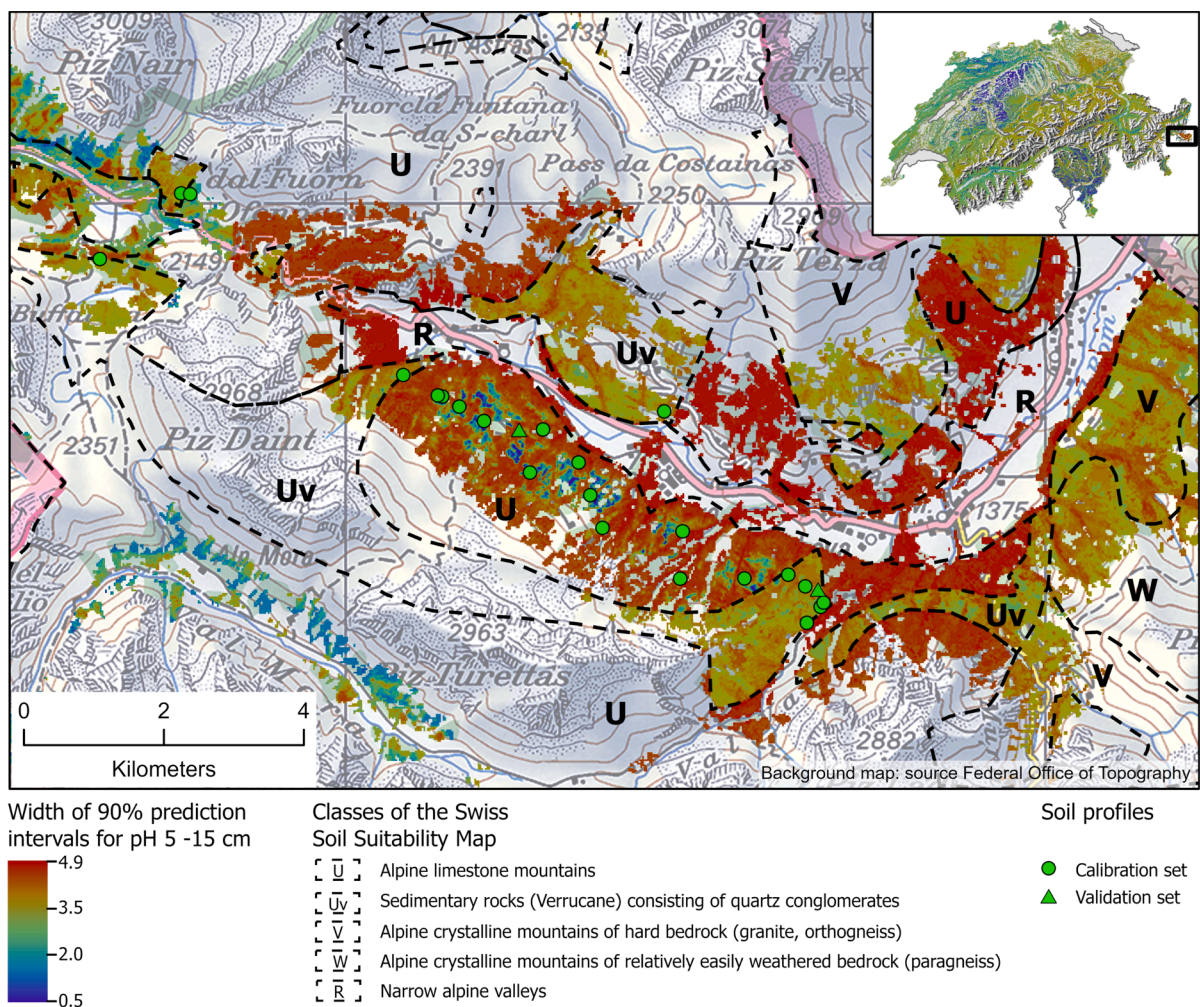- ● Calibration set
- ▲ Validation set

Fig. 9. Uncertainty map of pH (5–15 cm) for the Münstertal area. Within the class U of the Soil Suitability Map (Swiss Federal Statistical Office, 2001), the prediction interval and thus the uncertainty is higher than in the adjacent classes Uv and V.
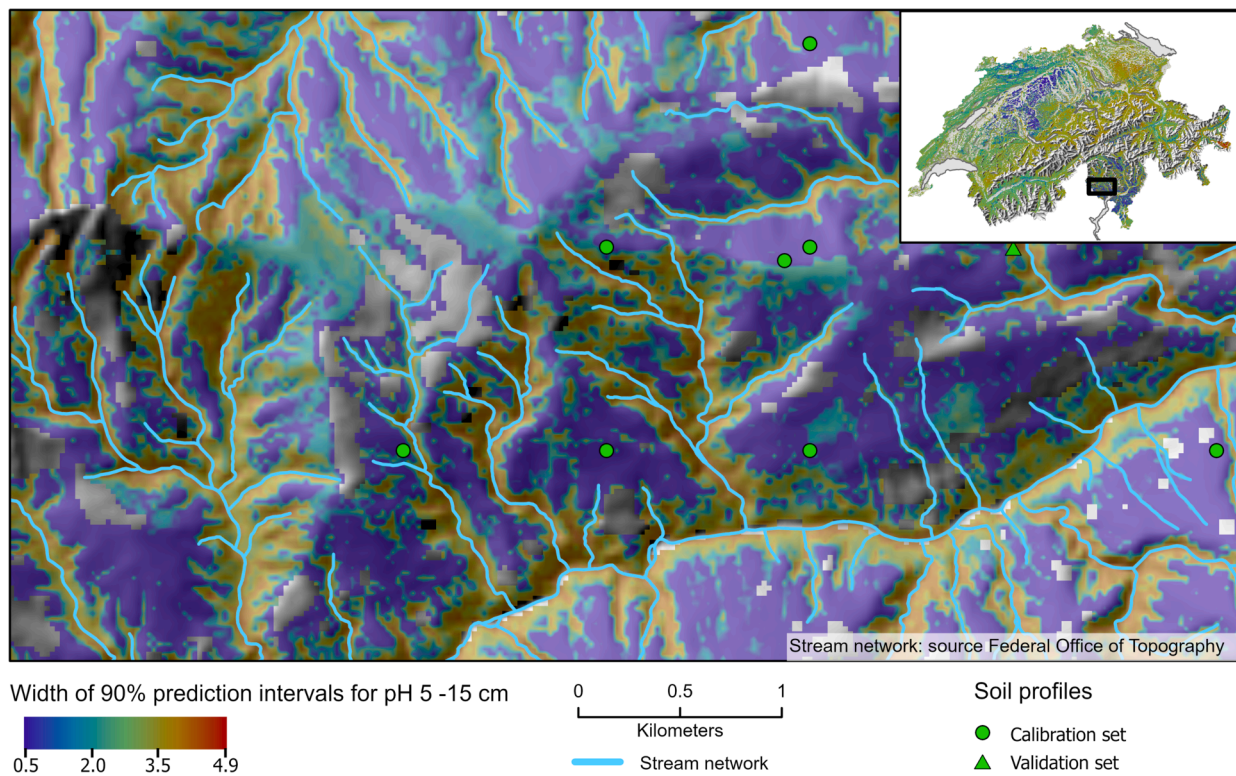
Fig. 10. Uncertainty map of pH (5–15 cm) for a region in the southern Swiss Alps. Large prediction interval widths (PI, high uncertainties) are associated with valleys while smaller PI are found on slopes and ridges.

map well reflects the general pattern of geology in Switzerland matching our expectations (Fig. 7). High pH-values (neutral to alkaline) were predicted in the Jura Mountains where Mesozoic limestones prevail. The Central Plateau is a Molasse basin filled with a mixture of calcareous and siliceous tertiary and quarternary sediments and therefore covers a wide range of pH values. In the Alps, the relation between predicted pH values and parent material is clearly visible, e.g. relatively high pH values in the inner Alpine valleys (west: Central Valais, east: Lower Engadine) with calcareous bedrock and low pH values in the upper Rhine valley (Surselva) with predominantly crystalline bedrock. The Southern Alps consist mainly of crystalline and metamorphic rocks and therefore have generally low pH values. Due to the high spatial resolution of the prediction and presumably also because of the multi-scale TAs, the map also well represents fine-scale pH variations. These plausible regional patterns correlate with topography and are particularly visible along ridges and valleys (Fig. 7, inset map).

Density plots comparing the range and distribution of observed and predicted pH values show that the models could not reproduce the bimodal distribution pattern of the measured pH values (Supplementary Fig. S2). However, the predicted pH generally increased with soil depth, which is in accordance with the theory of soil pedogenesis. For the other soil properties, the range and distribution of observed values were also not fully reproduced in the predictions (Supplementary Figs. S2, S3 and S4).

To assess the spatial pattern of uncertainty for this pH layer, we mapped the width of 90% PI computed by QRF (Fig. 8a). In general, the spatial patterns show large differences in PI widths across the forested area of Switzerland. Relatively small PI widths were found in the middle of the Central Plateau. This region largely coincides with the high sampling density of the soil profiles (Fig. 8b) and moreover, has relatively homogeneous and therefore uniformly acidified quaternary deposits.

The largest interval widths were found in the Münstertal (south-eastern corner of Switzerland, Fig. 8a and Fig. 9). Here, the prediction

uncertainty cannot be attributed to the profile density. It seems that the large uncertainty is due to the highly aggregated information and the coarse spatial delineation of the Swiss Soil Suitability Map (SSSM, Swiss Federal Statistical Office, 2001) that was used as a predictor. At the SSSM class boundaries between units "U" and "Uv" or "V", strong decreases in the interval width are evident. Whereas the unit "U" denotes "Alpine limestone mountains" and leads predominantly to alkaline soils, the unit "Uv" represents clastic sedimentary rocks (Verrucane) consisting of quartz conglomerates which lead to acidic soils. The latter also applies to the unit "V" which represents crystalline bedrock. The SSSM is unprecise in the Münstertal and overestimates the area of the unit "U" and therefore the pH is strongly overestimated in this unit. Although the SSSM does not adequately map the geological situation in the Münstertal region, overall it was an important covariate for our pH predictions. To improve the accuracy of pH modelling in this mountainous region, the description of the parent material needs to be improved. Similarly, Simon et al. (2020) showed for the Tyrolean Alps in Austria that detailed geological substrate information, including lithogenetic and mineralogical composition, is essential for digital soil mapping in mountainous areas.

Interestingly, in large parts of the Ticino (southern part of Switzerland, Fig. 10), the patterns of the PIs reflect the topography. Areas with small PI widths are found on the mountain slopes and ridges, and larger PIs in the valleys. Apparently, in this region the soil profiles were mainly sampled on the mountain slopes, but not in the valleys and led to these distinct patterns. In order to improve the prediction in the valleys, additional sampling sites should be chosen considering topography.

4. Conclusions

The primary objective of our study was to create high-resolution soil maps for a total of 37 target soil variables for the forested area of Switzerland. All statistical modelling methods used were able to deal

with the large number of potential covariates and selected the relevant variables efficiently with a minimum of user interaction. Model performances for the study area with its strong environmental gradients were variable and largely depended on the predicted soil property. When comparing the performances of the six modelling methods used, the differences were considerably smaller than they were between the predicted soil properties. In most cases, RF performed best and, contrary to our expectations, generally even outperformed MA. Although MA did not reduce the prediction variance in our study, we agree with Taghi-zadeh-Mehrjardi et al. (2019), that when using multiple algorithms, MA should always be tested and not simply the best performing one applied to make the prediction. It would be interesting to evaluate whether other weighting schemes such as Granger-Ramanathan or Bias-corrected Variance Weighted would have produced better predictive results. However, this would have required an additional calibration dataset to simultaneously retain the validation dataset for an independent assessment of the predictive performance.

Due to the only small differences in the performance of the modelling methods, we cannot give a clear recommendation as to which algorithm should generally be preferred to predict various soil properties. However, when only one method is used, RF proved to be a good choice. If RF is chosen for a DSM project, we strongly recommend the application of QRF, as this generalised form of RF can be used to calculate uncertainty maps in addition to the predicted soil maps. Uncertainty maps help to interpret models and their predictions which is crucial for machine learning algorithms to gain credibility (Wadoux et al., 2020). The spatial measure of uncertainty can also provide guidance for future sampling locations or in which region improved covariates (e.g. information about parent material) are needed.

Data availability

The QRF digital soil maps including the uncertainty maps are available via a map viewer: http://www.wsl.ch/soilmaps.

Declaration of Competing Interest

The authors declare that they have no known competing financial interests or personal relationships that could have appeared to influence the work reported in this paper.

Acknowledgements

Appendix A. Supplementary data

Supplementary data to this article can be found online at https://doi.org/10.1016/j.geodrs.2021.e00437.

References

Abbott, D., 2014. Applied Predictive Analytics: Principles and Techniques for the Professional Data Analyst. John Wiley & Sons, Incorporated, New York, USA.

Ågren, A.M., Larson, J., Paul, S.S., Laudon, H., Lidberg, W., 2021. Use of multiple LIDAR-derived digital terrain indices and machine learning for high-resolution national-scale soil moisture mapping of the Swedish forest landscape Geoderma, p. 404. https://doi.org/10.1016/j.geoderma.2021.115280.

AK SK (Arbeitskreis Standortskartierung), 2016. Forstliche Standortsaufnahme. Begriffe, Definitionen, Einteilungen, Kennzeichnungen, Erläuterungen, 7th edition. IHW-Verlag, München. 400 pp.

Araujo, M.B., New, M., 2007. Ensemble forecasting of species distributions. Trends Ecol. Evol. 22 (1), 42–47. https://doi.org/10.1016/j.tree.2006.09.010.

Arrouays, D., Grundy, M.G., Hartemink, A.E., Hempel, J.W., Heuvelink, G.B.M., Hong, S. Y., Lagacherie, P., Lelyk, G., McBratney, A.B., McKenzie, N.J., Mendonca-Santos, M. D.L., Minasny, B., Montanarella, L., Odeh, I.O.A., Sanchez, P.A., Thompson, J.A., Zhang, G.-L., 2014. GlobalSoilMap: toward a fine-resolution global grid of soil properties. Adv. Agron. 93–134.

Assami, T., Hamdi-Aissa, B., 2019. Digital mapping of soil classes in Algeria - a comparison of methods. Geoderma Reg 16. https://doi.org/10.1016/j.geodrs.2019.e00215.

Ballabio, C., 2009. Spatial prediction of soil properties in temperate mountain regions using support vector regression. Geoderma 151 (3–4), 338–350. https://doi.org/10.1016/j.geoderma.2009.04.022.

Baltensweiler, A., Walthert, L., Ginzler, C., Sutter, F., Purves, R.S., Hanewinkel, M., 2017. Terrestrial laser scanning improves digital elevation models and topsoil pH modelling in regions with complex topography and dense vegetation. Environ. Model Softw. 95, 13–21. https://doi.org/10.1016/j.envsoft.2017.05.009.

Baltensweiler, A., Heuvelink, G.B.M., Hanewinkel, M., Walthert, L., 2020. Microtopography shapes soil pH in flysch regions across Switzerland. Geoderma 380, 114663. https://doi.org/10.1016/j.geoderma.2020.114663.

Behrens, T., Zhu, A.X., Schmidt, K., Scholten, T., 2010. Multi-scale digital terrain analysis and feature selection for digital soil mapping. Geoderma 155 (3–4), 175–185. https://doi.org/10.1016/j.geoderma.2009.07.010.

Blackburn, G.A., 1998. Quantifying chlorophylls and Caroteniods at leaf and canopy scales: an evaluation of some Hyperspectral approaches. Remote Sens. Environ. 66 (3), 273–285. https://doi.org/10.1016/S0034-4257(98)00059-5.

Box, G.E.P., Cox, D.R., 1964. An analysis of transformations. J R Stat Soc B Methodol 26 (2), 211–243. https://doi.org/10.1111/j.2517-6161.1964.tb00553.x.

Brändli, U.B., Abegg, M., Allgaier Leuch, B., 2020. Schweizerisches Landesforstinventar. Ergebnisse der vierten Erhebung 2009-2017. Eidgenössische Forschungsanstalt für Wald, Schnee und Landschaft WSL; Bundesamt für Umwelt BAFU. Birmensdorf; Bern 341. https://doi.org/10.16904/envidat.146.

Bréda, N., Huc, R., Granier, A., Dreyer, E., 2006. Temperate forest trees and stands under severe drought: a review of ecophysiological responses, adaptation processes and long-term consequences. Ann. For. Sci. 63 (6), 625–644. https://doi.org/10.1051/forest:2006042.

Brungard, C.W., Boettinger, J.L., Duniway, M.C., Wills, S.A., Edwards, T.C., 2015. Machine learning for predicting soil classes in three semi-arid landscapes. Geoderma 239-240, 68–83. https://doi.org/10.1016/j.geoderma.2014.09.019.

Bundesamt für Landestopografie, 1967. Geotechnische Karte der Schweiz. https://opendata.swiss/de/dataset/geotechnische-karte-der-schweiz-1-200000 (last access: 06.03.2021).

Bundesamt für Raumentwicklung, 2016. Landschaftstypologie Schweiz. https://www.are.admin.ch/are/de/home/laendliche-raeume-und-berggebiete/grundlagen-und-daten/landschaftstypologie-schweiz.html (last access: 06.03.2021).

Buri, A., Grand, S., Yashiro, E., Adatte, T., Spangenberg, J.E., Pinto-Figueroa, E., Verrecchia, E., Guisan, A., 2020. What are the most crucial soil variables for predicting the distribution of mountain plant species? A comprehensive study in the Swiss Alps. J. Biogeogr. 47 (5), 1143–1153. https://doi.org/10.1111/jbi.13803.

Camathias, L., Bergamini, A., Kuchler, M., Stofer, S., Baltensweiler, A., 2013. High-resolution remote sensing data improves models of species richness. Appl. Veg. Sci. 16 (4), 539–551. https://doi.org/10.1111/avsc.12028.

Camera, C., Zomeni, Z., Noller, J.S., Zissimos, A.M., Christoforou, I.C., Bruggeman, A., 2017. A high resolution map of soil types and physical properties for Cyprus: a digital soil mapping optimization. Geoderma 285, 35–49. https://doi.org/10.1016/j.geoderma.2016.09.019.

Caubet, M., Román Dobarco, M., Arrouays, D., Minasny, B., Saby, N.P.A., 2019. Merging country, continental and global predictions of soil texture: lessons from ensemble modelling in France. Geoderma 337, 99–110. https://doi.org/10.1016/j.geoderma.2018.09.007.

Cavazzi, S., Corstanje, R., Mayr, T., Hannam, J., Fealy, R., 2013. Are fine resolution digital elevation models always the best choice in digital soil mapping? Geoderma 195-196 (0), 111–121. https://doi.org/10.1016/j.geoderma.2012.11.020.

Chen, S., Mulder, V.L., Heuvelink, G.B.M., Poggio, L., Caubet, M., Román Dobarco, M., Walter, C., Arrouays, D., 2020. Model averaging for mapping topsoil organic carbon in France. Geoderma 366, 114237. https://doi.org/10.1016/j.geoderma.2020.114237.

Creed, I.F., Trick, C.G., Band, L.E., Morrison, I.K., 2002. Characterizing the spatial pattern of soil carbon and nitrogen pools in the Turkey Lakes watershed: a comparison of regression techniques. Water, Air and Soil Pollution: Focus 2 (1), 81–102. https://doi.org/10.1023/A:1015886308016.

Davison, A.C., Hinkley, D.V., 1997. Bootstrap Methods and their Application. Cambridge university press.

Dharumarajan, S., Kalaiselvi, B., Suputhra, A., Lalitha, M., Hegde, R., Singh, S.K., Lagacherie, P., 2020. Digital soil mapping of key GlobalSoilMap properties in northern Karnataka plateau. Geoderma Reg 20. https://doi.org/10.1016/j.geodrs.2019.e00250.

Diks, C.G.H., Vrugt, J.A., 2010. Comparison of point forecast accuracy of model averaging methods in hydrologic applications. Stoch. Env. Res. Risk A. 24 (6), 809–820. https://doi.org/10.1007/s00477-010-0378-z.

Drusch, M., Del Bello, U., Carlier, S., Colin, O., Fernandez, V., Gascon, F., Hoersch, B., Isola, C., Laberinti, P., Martimort, P., Meygret, A., Spoto, F., Sy, O., Marchese, F., Bargellini, P., 2012. Sentinel-2: ESA's optical high-resolution Mission for GMES operational services. Remote Sens. Environ. 120, 25–36. https://doi.org/10.1016/j.rse.2011.11.026.

Freeman, T.G., 1991. Calculating catchment-area with divergent flow based on a regular grid. Comput. Geosci. 17 (3), 413–422. https://doi.org/10.1016/0098-3004(91)90048-I.

Frehner, M., Remund, J., Walthert, L., Kägi, M., Rihm, B., Brang, P., 2011. Schätzung standortspezifischer Trockenstressrisiken in Schweizer Wäldern. Schlussbericht / Version 2.3, Eidg. Forschungsanstalt für Wald, Schnee und Landschaft WSL. https://doi.org/10.3929/ethz-a-010693256.

Gal, Y., Ghahramani, Z., 2016. Dropout as a bayesian approximation: representing model uncertainty in deep learning, international conference on machine learning. PMLR 1050–1059.

Gee, G.W., Bauder, J., Klute, A., 1986. Methods of soil analysis, part 1, physical and mineralogical methods. Soil science Society of America Book Series. American Society of Agronomy, Inc. and Soil Science Society of America, Inc. Madison, Wisconsin, pp. 404–410.

Gitelson, A.A., Kaufman, Y.J., Merzlyak, M.N., 1996. Use of a green channel in remote sensing of global vegetation from EOS-MODIS. Remote Sens. Environ. 58 (3), 289–298. https://doi.org/10.1016/S0034-4257(96)00072-7.

Gomes, L.C., Faria, R.M., de Souza, E., Veloso, G.V., Schaefer, C.E.G.R., Filho, E.I.F., 2019. Modelling and mapping soil organic carbon stocks in Brazil. Geoderma 340, 337–350. https://doi.org/10.1016/j.geoderma.2019.01.007.

Gonseth, Y., Wohlgemuth, T., Sansonnens, B., Buttler, A., 2001. Die biogeographischen Regionen der Schweiz. Erläuterungen und Einteilungsstandard. Umwelt Materialien Nr. 137. Swiss Agency for the Environment, Forests and Landscape SAEFL, Bern.

Goovaerts, P., 2001. Geostatistical modelling of uncertainty in soil science. Geoderma 103 (1), 3–26. https://doi.org/10.1016/S0016-7061(01)00067-2.

Greiner, L., Keller, A., Gret-Regamey, A., Papritz, A., 2017. Soil function assessment: review of methods for quantifying the contributions of soils to ecosystem services. Land Use Policy 69, 224–237. https://doi.org/10.1016/j.landusepol.2017.06.025.

Grinand, C., Arrouays, D., Laroche, B., Martin, M.P., 2008. Extrapolating regional soil landscapes from an existing soil map: sampling intensity, validation procedures, and integration of spatial context. Geoderma 143 (1–2), 180–190. https://doi.org/10.1016/j.geoderma.2007.11.004.

Grunwald, S., Thompson, J.A., Boettinger, J.L., 2011. Digital soil mapping and modeling at continental scales: finding solutions for global issues. Soil Sci. Soc. Am. J. 75 (4), 1201–1213. https://doi.org/10.2136/sssaj2011.0025.

Guevara, M., Olmedo, G.F., Stell, E., Yigini, Y., Aguilar Duarte, Y., Arellano Hernández, C., Arévalo, G.E., Arroyo-Cruz, C.E., Bolivar, A., Bunning, S., Bustamante Cañas, N., Cruz-Gaistardo, C.O., Davila, F., Dell Acqua, M., Encina, A., Figueredo Tacona, H., Fontes, F., Hernández Herrera, J.A., Ibelles Navarro, A.R., Loayza, V., Manueles, A.M., Mendoza Jara, F., Olivera, C., Osorio Hermosilla, R., Pereira, G., Prieto, P., Ramos, I.A., Rey Brina, J.C., Rivera, R., Rodríguez-Rodríguez, J., Roopnarine, R., Rosales Ibarra, A., Rosales Riveiro, K.A., Schulz, G.A., Spence, A., Vasques, G.M., Vargas, R.R., Vargas, R., 2018. No silver bullet for digital soil mapping: country-specific soil organic carbon estimates across Latin America. SOIL 4 (3), 173–193. https://doi.org/10.5194/soil-4-173-2018.

Guo, Z., Xiao, X., Gan, Y., Zheng, Y., 2001. Ecosystem functions, services and their values – a case study in Xingshan County of China. Ecol. Econ. 38 (1), 141–154. https://doi.org/10.1016/S0921-8009(01)00154-9.

Hamzehpour, N., Shafizadeh-Moghadam, H., Valavi, R., 2019. Exploring the driving forces and digital mapping of soil organic carbon using remote sensing and soil texture. Catena 182, 104141. https://doi.org/10.1016/j.catena.2019.104141.

Hartanto, H., Prabhu, R., Widayat, A.S.E., Asdak, C., 2003. Factors affecting runoff and soil erosion: plot-level soil loss monitoring for assessing sustainability of forest management. For. Ecol. Manag. 180 (1–3), 361–374. https://doi.org/10.1016/s0378-1127(02)00656-4.

Hartmann, M., Howes, C.G., VanInsberghe, D., Yu, H., Bachar, D., Christen, R., Henrik Nilsson, R., Hallam, S.J., Mohn, W.W., 2012. Significant and persistent impact of timber harvesting on soil microbial communities in northern coniferous forests. ISME J 6 (12), 2199–2218. https://doi.org/10.1038/ismej.2012.84.

Hastie, T., Tibshirani, R., Friedman, J., 2009. The Elements of Statistical Learning. Springer Series in Statistics, 2 nd ed. Springer New York.

Hengl, T., Nussbaum, M., Wright, M.N., Heuvelink, G.B.M., Graler, B., 2018. Random forest as a generic framework for predictive modeling of spatial and spatio-temporal variables. PeerJ 6, e5518. https://doi.org/10.7717/peerj.5518.

Hertzog, M., 2017. Modelling Soil Attributes with the Random Forest Method for the Swiss Forest Area. Master Thesis, ETH Zurich, 75 pp.

Heung, B., Hodul, M., Schmidt, M.G., 2017. Comparing the use of training data derived from legacy soil pits and soil survey polygons for mapping soil classes. Geoderma 290, 51–68. https://doi.org/10.1016/j.geoderma.2016.12.001.

Hoffmann, U., Hoffmann, T., Johnson, E.A., Kuhn, N.J., 2014. Assessment of variability and uncertainty of soil organic carbon in a mountainous boreal forest (Canadian Rocky Mountains, Alberta). CATENA 113, 107–121. https://doi.org/10.1016/j.catena.2013.09.009.

Hümann, M., Schüler, G., Müller, C., Schneider, R., Johst, M., Caspari, T., 2011. Identification of runoff processes – the impact of different forest types and soil properties on runoff formation and floods. J. Hydrol. 409 (3–4), 637–649. https://doi.org/10.1016/j.jhydrol.2011.08.067.

Jenness, J., 2011. Topographic Position Index (TPI) v. 1.2. http://www.jennessent.com. last access: 17.03.2021.

Kasraei, B., Heung, B., Saurette, D.D., Schmidt, M.G., Bulmer, C.E., Bethel, W., 2021. Quantile regression as a generic approach for estimating uncertainty of digital soil maps produced from machine-learning. Environ. Model Softw. 144, 105139. https://doi.org/10.1016/j.envsoft.2021.105139.

Keskin, H., Grunwald, S., Harris, W.G., 2019. Digital mapping of soil carbon fractions with machine learning. Geoderma 339, 40–58. https://doi.org/10.1016/j.geoderma.2018.12.037.

Kim, D., Zheng, Y.B., 2011. Scale-dependent predictability of DEM-based landform attributes for soil spatial variability in a coastal dune system. Geoderma 164 (3–4), 181–194. https://doi.org/10.1016/j.geoderma.2011.06.002.

Kuhn, M., Johnson, K., 2013. Applied Predictive Modeling, 26. Springer.

Lal, R., 2005. Forest soils and carbon sequestration. For. Ecol. Manag. 220 (1–3), 242–258. https://doi.org/10.1016/j.foreco.2005.08.015.

Liaw, A., Wiener, M., 2002. Classification and regression by randomForest. R News 2 (3), 18–22.

Liddicoat, C., Maschmedt, D., Clifford, D., Searle, R., Herrmann, T., Macdonald, L.M., Baldock, J., 2015. Predictive mapping of soil organic carbon stocks in South Australia's agricultural zone. Soil Research 53 (8). https://doi.org/10.1071/sr15100.

Liu, F., Zhang, G.-L., Song, X., Li, D., Zhao, Y., Yang, J., Wu, H., Yang, F., 2020. High-resolution and three-dimensional mapping of soil texture of China. Geoderma 361, 114061. https://doi.org/10.1016/j.geoderma.2019.114061.

Mahmoudzadeh, H., Matinfar, H.R., Taghizadeh-Mehrjardi, R., Kerry, R., 2020. Spatial prediction of soil organic carbon using machine learning techniques in western Iran. Geoderma Reg 21, e00260. https://doi.org/10.1016/j.geodrs.2020.e00260.

Malone, B.P., McBratney, A.B., Minasny, B., 2011. Empirical estimates of uncertainty for mapping continuous depth functions of soil attributes. Geoderma 160 (3–4), 614–626. https://doi.org/10.1016/j.geoderma.2010.11.013.

Malone, B.P., Minasny, B., Odgers, N.P., McBratney, A.B., 2014. Using model averaging to combine soil property rasters from legacy soil maps and from point data. Geoderma 232-234, 34–44. https://doi.org/10.1016/j.geoderma.2014.04.033.

Masek, J.G., Vermote, E.F., Saleous, N.E., Wolfe, R., Hall, F.G., Huemmrich, K.F., Feng, G., Kutler, J., Teng-Kui, L., 2006. A Landsat surface reflectance dataset for North America, 1990-2000. IEEE Geosci. Remote Sens. Lett. 3 (1), 68–72. https://doi.org/10.1109/LGRS.2005.857030.

Maynard, J.J., Johnson, M.G., 2014. Scale-dependency of LiDAR derived terrain attributes in quantitative soil-landscape modeling: effects of grid resolution vs. neighborhood extent. Geoderma 230 (0), 29–40. https://doi.org/10.1016/j.geoderma.2014.03.021.

McBratney, A.B., Santos, M.L.M., Minasny, B., 2003. On digital soil mapping. Geoderma 117 (1–2), 3–52. https://doi.org/10.1016/S0016-7061(03)00223-4.

McDowell, N.G., Allen, C.D., Anderson-Teixeira, K., Aukema, B.H., Bond-Lamberty, B., Chini, L., Clark, J.S., Dietze, M., Grossiord, C., Hanbury-Brown, A., Hurtt, G.C., Jackson, R.B., Johnson, D.J., Kueppers, L., Lichstein, J.W., Ogle, K., Poulter, B., Pugh, T.A.M., Seidl, R., Turner, M.G., Uriarte, M., Walker, A.P., Xu, C., 2020. Pervasive shifts in forest dynamics in a changing world. Science 368 (6494). https://doi.org/10.1126/science.aaz9463.

Meinshausen, N., 2006. Quantile regression forests. J. Mach. Learn. Res. 7, 983–999.

Meinshausen, N., 2017. quantregForest: Quantile Regression Forests. https://CRAN.R-project.org/package=quantregForest.

MeteoSwiss, 2020. Spatial Climate Analyses. https://www.meteoswiss.admin.ch/home/climate/swiss-climate-in-detail/raeumliche-klimaanalysen.html (last access: 25.08.2020).

Miller, B.A., Koszinski, S., Wehrhan, M., Sommer, M., 2015. Impact of multi-scale predictor selection for modeling soil properties. Geoderma 239, 97–106. https://doi.org/10.1016/j.geoderma.2014.09.018.

Minasny, B., McBratney, A.B., 2016. Digital soil mapping: a brief history and some lessons. Geoderma 264, 301–311. https://doi.org/10.1016/j.geoderma.2015.07.017.

Mod, H.K., Scherrer, D., Luoto, M., Guisan, A., Scheiner, S., 2016. What we use is not what we know: environmental predictors in plant distribution models. J. Veg. Sci. 27 (6), 1308–1322. https://doi.org/10.1111/jvs.12444.

Møller, A.B., Beucher, A.M., Pouladi, N., Greve, M.H., 2020. Oblique geographic coordinates as covariates for digital soil mapping. SOIL 6 (2), 269–289. https://doi.org/10.5194/soil-6-269-2020.

Mosimann, T., 2004-2010. Dokumentation der Waldböden der Kantone Basel-Landschaft und Basel-Stadt. Geosynthesis Sonderbände 1–4; Physische Geographie und Landschaftsökologie, Leibniz Universität Hannover; erarbeitet im Auftrag des Amts für Umweltschutz und Energie des Kantons Basel-Landschaft sowie des Forstamts beider Basel.

Motiejūnaitė, J., Børja, I., Ostonen, I., Bakker, M.R., Bjarnadottir, B., Brunner, I., Iršėnaitė, R., Mrak, T., Oddsdóttir, E.S., Lehto, T., 2019. Cultural ecosystem services provided by the biodiversity of forest soils: a European review. Geoderma 343, 19–30. https://doi.org/10.1016/j.geoderma.2019.02.025.

Mulder, V.L., de Bruin, S., Schaepman, M.E., Mayr, T.R., 2011. The use of remote sensing in soil and terrain mapping - a review. Geoderma 162 (1–2), 1–19. https://doi.org/10.1016/j.geoderma.2010.12.018.

Mulder, V.L., Lacoste, M., Richer-de-Forges, A.C., Arrouays, D., 2016. GlobalSoilMap France: high-resolution spatial modelling the soils of France up to two meter depth. Sci. Total Environ. 573, 1352–1369. https://doi.org/10.1016/j.scitotenv.2016.07.066.

Nussbaum, M., Papritz, A., Baltensweiler, A., Walthert, L., 2014. Estimating soil organic carbon stocks of Swiss forest soils by robust external-drift kriging. Geosci. Model Dev. 7 (3), 1197–1210. https://doi.org/10.5194/gmd-7-1197-2014.

Nussbaum, M., Papritz, A., Zimmermann, S., Walthert, L., 2016. Pedotransfer function to predict density of forest soils in Switzerland. J. Plant Nutr. Soil Sci. 179 (3), 321–326. https://doi.org/10.1002/jpln.201500546.

Nussbaum, M., Spiess, K., Baltensweiler, A., Grob, U., Keller, A., Greiner, L., Schaepman, M.E., Papritz, A., 2018. Evaluation of digital soil mapping approaches with large sets of environmental covariates. Soil 4 (1), 1–22. https://doi.org/10.5194/soil-4-1-2018.

O'Callaghan, J.F., Mark, D.M., 1984. The extraction of drainage networks from digital elevation data. Computer Vision, Graphics, and Image Processing 28 (3), 323–344. https://doi.org/10.1016/s0734-189x(84)80011-0.

Padarian, J., Minasny, B., McBratney, A.B., 2017. Chile and the Chilean soil grid: a contribution to GlobalSoilMap. Geoderma Reg 9, 17–28. https://doi.org/10.1016/j.geodrs.2016.12.001.

Pereira, P., Bogunovic, I., Muñoz-Rojas, M., Brevik, E.C., 2018. Soil ecosystem services, sustainability, valuation and management. Current Opinion in Environmental Science & Health 5, 7–13. https://doi.org/10.1016/j.coesh.2017.12.003.

Petermann, E., Meyer, H., Nussbaum, M., Bossew, P., 2021. Mapping the geogenic radon potential for Germany by machine learning. Sci. Total Environ. 754, 142291. https://doi.org/10.1016/j.scitotenv.2020.142291.

Román Dobarco, M., Arrouays, D., Lagacherie, P., Ciampalini, R., Saby, N.P.A., 2017. Prediction of topsoil texture for region Centre (France) applying model ensemble methods. Geoderma 298, 67–77. https://doi.org/10.1016/j.geoderma.2017.03.015.

Rouse, J.W., Haas, R.H., Schell, J.A., Deering, D.W., 1974. Monitoring vegetation systems in the Great Plains with ERTS. In: Freden, S.C., Mercanti, E.P., Becker, M.A. (Eds.), Third Earth Resource Technology Satellite (ERTS) Symposium. National Aeronautics and Space Administration, NASA SP-351, Washington D.C., pp. 309–317.

Scherrer, D., Guisan, A., 2019. Ecological indicator values reveal missing predictors of species distributions. Sci. Rep. 9 (1), 3061. https://doi.org/10.1038/s41598-019-39133-1.

Seibert, J., Stendahl, J., Sorensen, R., 2007. Topographical influences on soil properties in boreal forests. Geoderma 141 (1–2), 139–148. https://doi.org/10.1016/j.geoderma.2007.05.013.

Simon, A., Geitner, C., Katzensteiner, K., 2020. A framework for the predictive mapping of forest soil properties in mountain areas. Geoderma 371, 114383. https://doi.org/10.1016/j.geoderma.2020.114383.

Spiess, K., 2016. Vorhersage von Bodeneigenschaften mit Quantile Regression Forest, Validierung und Vergleich mit den Vorhersagen aus geoadditiven Modellen. Bsc Thesis, ETH Zurich, Switzerland.

Swiss Federal Statistical Office, 2001. Swiss soil suitability map. https://www.bfs.admin.ch/bfs/en/home/services/geostat/swiss-federal-statistics-geodata/land-use-cover-suitability/derivative-complementary-data/swiss-soil-suitability-map.html (last access: 06.03.2021).

Swiss National Forest Inventory LFI, 1984. PH Topsoil Samples from the Swiss National Forest Inventory. Swiss Federal Institute for Forest. Snow and Landscape Research WSL, Birmensdorf.

Swisstopo, 2007. Hydrogeological Map of Switzerland. https://www.swisstopo.admin.ch/en/geodata/geology/maps/gk500/raster.html#download (last access: 06.03.2021).

Swisstopo, 2009. Switzerland during the Last Glacial Maximum. https://www.swisstopo.admin.ch/en/geodata/geology/maps/gk500/raster.html#download (last access: 06.03.2021).

Swisstopo, 2020. Height Models. https://www.swisstopo.admin.ch/en/geodata/height.html (last access: 06.03.2021).

Szatmári, G., Pásztor, L., 2019. Comparison of various uncertainty modelling approaches based on geostatistics and machine learning algorithms. Geoderma 337, 1329–1340. https://doi.org/10.1016/j.geoderma.2018.09.008.

Taghizadeh-Mehrjardi, R., Minasny, B., Toomanian, N., Zeraatpisheh, M., Amirian-Chakan, A., Triantafilis, J., 2019. Digital mapping of soil classes using Ensemble of Models in Isfahan region, Iran. Soil Systems 3 (2), 37.

Tebaldi, C., Knutti, R., 2007. The use of the multi-model ensemble in probabilistic climate projections. Philos. Trans. R. Soc. A Math. Phys. Eng. Sci. 365 (1857), 2053–2075. https://doi.org/10.1098/rsta.2007.2076.

Thomas, M., Clifford, D., Bartley, R., Philip, S., Brough, D., Gregory, L., Willis, R., Glover, M., 2015. Putting regional digital soil mapping into practice in tropical northern Australia. Geoderma 241-242, 145–157. https://doi.org/10.1016/j.geoderma.2014.11.016.

Vaysse, K., Lagacherie, P., 2015. Evaluating digital soil mapping approaches for mapping GlobalSoilMap soil properties from legacy data in Languedoc-Roussillon (France). Geoderma Reg 4, 20–30. https://doi.org/10.1016/j.geodrs.2014.11.003.

Vaysse, K., Lagacherie, P., 2017. Using quantile regression forest to estimate uncertainty of digital soil mapping products. Geoderma 291, 55–64. https://doi.org/10.1016/j.geoderma.2016.12.017.

Viscarra Rossel, R.A., Chen, C., Grundy, M.J., Searle, R., Clifford, D., Campbell, P.H., 2015. The Australian three-dimensional soil grid: Australia's contribution to the GlobalSoilMap project. Soil Research 53 (8), 845–864. https://doi.org/10.1071/SR14366.

Wadoux, A.M.J.C., 2019. Using deep learning for multivariate mapping of soil with quantified uncertainty. Geoderma 351, 59–70. https://doi.org/10.1016/j.geoderma.2019.05.012.

Wadoux, A.M.J.C., Minasny, B., McBratney, A.B., 2020. Machine learning for digital soil mapping: applications, challenges and suggested solutions. Earth Sci. Rev. 210 https://doi.org/10.1016/j.earscirev.2020.103359.

Walthert, L., Zimmermann, S., Blaser, P., Luster, J., Lüscher, P., 2004. Waldböden der Schweiz. In: Grundlagen und Region Jura, Band 1. Forschungsanstalt WSL, Hep Verlag, Birmensdorf, Bern, Eidg.

Walthert, L., Graf, U., Kammer, A., Luster, J., Pezzotta, D., Zimmermann, S., Hagedorn, F., 2010. Determination of organic and inorganic carbon, δ13C, and nitrogen in soils containing carbonates after acid fumigation with HCl. J. Plant Nutr. Soil Sci. 173 (2), 207–216. https://doi.org/10.1002/jpln.200900158.

Walthert, L., Scherler, M., Stähli, M., Huber, M., Baltensweiler, A., Ramirez-Lopez, L., Papritz, A., 2015. Böden und Wasserhaushalt von Wäldern und Waldstandorten der Schweiz unter heutigem und zukünftigem Klima (BOWA-CH). Birmensdorf. https://doi.org/10.3929/ethz-a-010658682.

Waser, L.T., Ginzler, C., Rehush, N., 2017. Wall-To-Wall tree type mapping from countrywide airborne remote sensing surveys. Remote Sens. 9 (8), 766. https://doi.org/10.3390/rs9080766.

Wei, L.J., 1992. The accelerated failure time model: a useful alternative to the Cox regression model in survival analysis. Stat. Med. 11 (14–15), 1871–1879. https://doi.org/10.1002/sim.4780111409.

Wilks, D.S., 2011. Statistical Methods in the Atmospheric Sciences, 100. Academic press.

Yang, R.-M., Zhang, G.-L., Liu, F., Lu, Y.-Y., Yang, F., Yang, F., Yang, M., Zhao, Y.-G., Li, D.-C., 2016. Comparison of boosted regression tree and random forest models for mapping topsoil organic carbon concentration in an alpine ecosystem. Ecol. Indic. 60, 870–878. https://doi.org/10.1016/j.ecolind.2015.08.036.

Zimmermann, N.E., Kienast, F., 1999. Predictive mapping of alpine grasslands in Switzerland: species versus community approach. J. Veg. Sci. 10, 469–482.